Research Article | Vol. 28, No. 10 / 11 May 2020 / Optics Express 14638
Optics EXPRESS

Low-noise distributed acoustic sensing using enhanced backscattering fiber with ultra-low-loss point reflectors

Brandon Redding,[1,*] Matthew J. Murray,[1] Andrei Donko,[2] Martynas Beresna,[2] Ali Masoudi,[2] and Gilberto Brambilla[2]

[1] Optical Sciences Division, U.S. Naval Research Laboratory, 4555 Overlook Ave. SW, Washington, D.C. 20375, USA
[2] Optoelectronics Research Centre, University of Southampton, Southampton SO17 1BJ, UK
[*] brandon.redding@nrl.navy.mil

Abstract: We present a low-noise distributed acoustic sensor using enhanced backscattering fiber with a series of localized reflectors. The point reflectors were inscribed in a standard telecom fiber in a fully automated system by focusing an ultra-fast laser through the fiber cladding. The inscribed reflectors provided a reflectance of −53 dB, significantly higher than the Rayleigh backscattering level of −70 dB/m, despite adding only 0.01 dB of loss per 100 reflection points. We constructed a coherent φ-OTDR system using a double-pulse architecture to probe the enhanced backscattering fiber. Using this system, we found that the point reflectors enabled an average phase noise of −91 dB (re rad^2/Hz), 20 dB lower than sensors formed using Rayleigh backscattering in the same fiber. The sensors are immune to interference fading, exhibit a high degree of linearity, and demonstrate excellent non-local signal suppression (>50 dB). This work illustrates the potential for low-cost enhanced backscattering fiber to enable low-noise, long-range distributed acoustic sensing.

1. Introduction

Distributed acoustic sensors (DAS) based on coherent phase-sensitive optical time-domain reflectometry (φ-OTDR) are attractive due to their ability to perform distributed, dynamic strain measurements over long distances using commercial-off-the-shelf fiber [1]. As a result, DAS systems have been used for a variety of applications, including perimeter intrusion detection [2], pipeline monitoring [3], subsea cable condition analysis [4] and structural health monitoring [1]. Despite their success, coherent φ-OTDR sensors have two significant limitations. First, these sensors rely on collecting Rayleigh backscattered light, which is an inherently weak process, leading to low light levels that limit the sensitivity of these systems. While increasing the input power could compensate for such low reflectance, non-linear thresholds limit the power that can be injected into the fiber. Second, these sensors are susceptible to polarization and interference fading [5–7]. Although frequency and polarization multiplexing can address this issue, these techniques increase the system cost and complexity [8,9].

Recently, a number of groups have proposed novel interrogation techniques to address these limitations in an on-going effort to achieve lower noise Rayleigh-based DAS [10–13]. While these works are promising, the interrogation systems are considerably more complex, often requiring high-speed modulators and detectors, or increased computational processing. As an alternative, researchers have recently proposed modifying the fiber itself in order to realize lower noise DAS. These fiber-modification efforts can by divided into two approaches. The first approach relies

#389212 https://doi.org/10.1364/OE.389212
Journal © 2020 Received 28 Jan 2020; revised 9 Apr 2020; accepted 22 Apr 2020; published 29 Apr 2020

Optics EXPRESS

on increasing the distributed backscattering throughout the fiber. This can be accomplished by exposing hydrogen-loaded fiber to UV light [14] or by using an ultra-fast laser to inscribe scattering defects along the length of the fiber [15]. Alternatively, researchers have proposed introducing continuous random fiber Bragg grating (FBG) [16,17] or overlapping a series of chirped FBGs [18,19] to provide continuously enhanced backscattering without the narrow bandwidth that would typically be associated with a long FBG. While these approaches have shown promise in relatively short-range applications (typically <100 m), a continuous increase in the backscattering coefficient is accompanied by significantly higher attenuation which can limit the sensing range. To address this, researchers have suggested using a limited length of this type of continuously enhanced backscattering fiber after long lengths of standard fiber to achieve long-range sensing without accruing additional loss over the entire fiber under test [20]. The second approach is to increase the reflectivity at a series of discrete locations in the fiber. Since discrete reflectors only increase the attenuation at specific locations, longer range sensing is still possible as long as the reflectance is sufficiently low. In addition, this approach has the potential to eliminate interference fading. Researchers initially suggested using ultra-weak fiber Bragg gratings as discrete reflectors [21–24]; however, FBGs operate in a relatively narrow band and the fabrication of consistent low-reflectance FBGs is extremely challenging [25]. Recently, an alternative approach was proposed using an ultra-fast laser to inscribe low-reflectivity point defects through the fiber cladding [26,27]. This technique is compatible with standard telecom fiber, providing a potentially scalable path to introduce discrete reflectors in long lengths of fiber. However, quantitative measurements confirming that this type of point reflector can be used for low-noise distributed strain sensing have not been reported to our knowledge.

In this work, we present a low-noise DAS using enhanced backscattering fiber (EBF) with a series of localized point reflectors. The reflection points were inscribed in standard telecom fiber using a custom-built apparatus. Using this apparatus, we added a series of localized reflectors spaced by 20 m with an average reflectance of −53 dB. We found that 100 reflectors introduced less than 0.01 dB of attenuation, making this approach compatible with long-range strain sensing. We then constructed a coherent φ-OTDR system using a double-pulse scheme to compare the sensor performance using the localized reflectors with the performance using Rayleigh backscattered light. We measured an average phase noise of −91 dB (re rad^2/Hz) using the point reflectors compared with an average phase noise of −69 dB (re rad^2/Hz) using the Rayleigh backscattered light in the same measurement. The sensor formed with the point reflectors exhibited the same sensitivity to strain as a standard Rayleigh based measurement, a high degree of linearity, and excellent non-local signal suppression. We also found that the sensors formed using point reflectors were immune to interference fading, enabling a simplified interrogation system. This work confirms that localized point reflectors can significantly improve the sensitivity of DAS based on a standard coherent φ-OTDR architecture.

2. Fiber design and fabrication

A fully automated fiber inscription setup was constructed to introduce the point reflectors. A schematic of the inscription setup is shown in Fig. 1(a). A Yb:KGW (ytterbium-doped potassium gadolinium tungstate) laser with a pulse duration of 206 fs was frequency doubled to 515 nm and focused onto the fiber. A 3D printed stage was used to align the fiber at the focal point of the laser while it was fed between two spools. This technique is capable of inserting localized reflection points in km-length spools of standard telecom fiber without removing the fiber coating (which is transparent at the laser wavelength). A schematic of the EBF is shown in Fig. 1(b). The sensor position and size are defined by the spacing between the localized point reflectors. In this proof-of-concept demonstration, we separated the point reflectors by 20 m, allowing us to wind part of the fiber between the reflectors on a piezo-electric transducer (PZT) cylinder in order to characterize the responsivity of the sensor. The measured reflectance is shown in

Optics EXPRESS

Fig. 1(c). In this measurement, the fiber under test consisted of ~500 m of standard telecom fiber (Corning SMF-28e) followed by 200 m of EBF with 10 reflectors spaced by 20 m. The point reflectors had an average reflectance of −53 dB. Note that this reflectance was independent of pulse duration, in contrast to the Rayleigh backscattering signal which increases with pulse duration and is approximately −70 dB/m for standard telecom fiber.

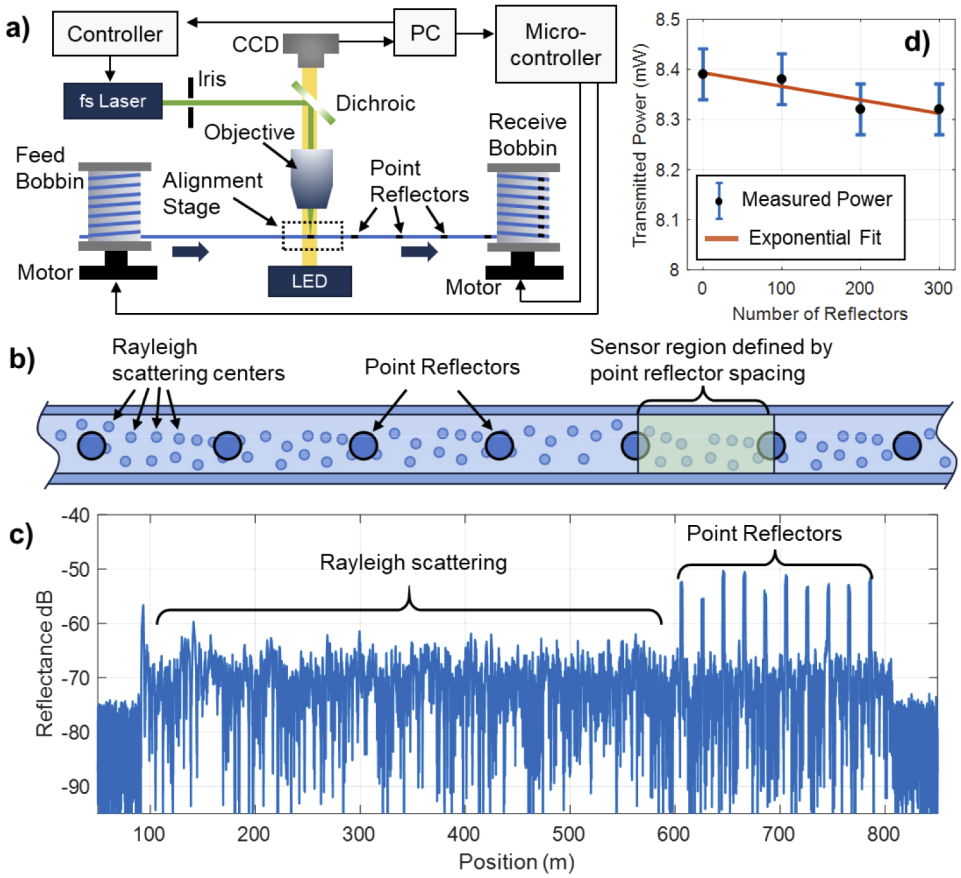

Fig. 1. (a) Schematic of the reel-to-reel, automated, fiber inscription set up. A femtosecond laser was directed onto the fiber through an iris, a dichroic mirror and an objective lens. A 3D printed stage was used to position the fiber under the objective lens and a LED and camera were used to monitor the fiber alignment. A PC and microcontroller were used to manage the process. (b) Schematic of the EBF. A series of localized point reflectors were inscribed in standard single mode fiber. The sensor region is defined by the spacing between the localized reflectors. (c) Reflectance measurement using an EBF with 10 reflectors spaced by 20 m. The localized reflectors had an average reflectance of −53 dB.

In order to evaluate the attenuation introduced by the point reflectors, we performed a cut-back measurement on a separate fiber containing 300 point reflectors. The reflectors were fabricated with the same parameters as those used in the dynamic strain measurement reported in this work. The reflectors were divided into three sections containing 100 reflectors each, with 2 meters of fiber between each section. Within each section, the spacing between the reflectors was randomized to avoid any interference effects. The fiber was connectorized with APC pigtails at both ends. To measure the loss, a continuous 1550 nm source was launched into the fiber and the transmitted power was recorded using a photodiode. This measurement was then repeated

Optics EXPRESS

after sequentially removing each of the 100-reflector fiber sections and re-splicing the fiber. The results of the cutback measurement are shown in Fig. 1(d). Note that the attenuation of the 100-reflector segments is comparable to the loss induced by the splices. Although this introduces some uncertainty, we were able to estimate the attenuation by fitting the decrease in transmitted power with increasing reflectors, as shown in Fig. 1(d). This fit indicated that the reflectors introduced ~0.01 dB of loss per 100 reflectors.

The reflectance of the sample tested in this work strikes a balance between providing higher return light levels than Rayleigh backscattering and introducing excessive attenuation or introducing significant levels of cross-talk which could build up in a fiber with many point reflectors [28]. In general, the optimal reflectance will depend on the total fiber length and sensor spacing required for a given application along with the acceptable level of cross-talk. Nonetheless, this sample is sufficient for our purpose of confirming that this type of point reflector enables low noise strain sensing without compromising the linearity or non-local signal rejection of Rayleigh-based coherent φ-OTDR systems.

3. Interrogation system

We constructed a coherent φ-OTDR system to interrogate the EBF. We adopted a double-pulse interrogation scheme due to its reduced sensitivity to laser phase noise and excellent non-local signal rejection. A narrow-line seed laser was carved into 20 ns pulses using a combination of an electro-optic modulator (EOM) and acousto-optic modulator (AOM). The EOM generated 20 ns pulses with modest extinction (~20 dB) while the AOM generated 150 ns pulses with high extinction (~50 dB). This resulted in a 20 ns-wide pulse with a 150 ns-wide pedestal and high extinction outside the pedestal. The pulse repetition rate was set to 100 kHz. The pulses were then directed to a path-mismatched interferometer with an AOM in each arm. The AOMs were driven at 55 MHz and 55.025 MHz. The pulses in the two arms were delayed by 40 m and had a relative frequency offset of 25 kHz. The delay line was selected to match the round-trip distance between the point reflectors, allowing us to form sensors using light reflected from neighboring reflectors. The intermediate frequency between the pulses was used as a carrier, allowing us to recover the relative phase between the two pulses. The pulse pair was then amplified to a peak power of 500 mW using an erbium-doped fiber amplifier (EDFA) and the amplified spontaneous emission (ASE) was removed using a 100 GHz wide wavelength division multiplexing (WDM) filter. The pulses were then injected into the fiber under test (FUT). Approximately 1 m of fiber was wrapped on a PZT between the 8^{th} and 9^{th} point reflectors to introduce a test signal. The Rayleigh backscattered light along with the light from the point reflectors were amplified using a second EDFA, filtered, and directed to a polarization diversity receiver, which helped to minimize polarization fading. The interference signal between the two pulses was recorded on a pair of 150 MHz photodetectors and digitized at 5 GS/s.

This scheme allowed the interrogation system to measure the relative phase between the two pulses as a function of position in the fiber. In other words, the system measured the relative phase between light backscattered from a pair of 2 m reflector regions separated by 20 m. The 2 m reflector region size was set by the 20 ns pulse duration, while the 20 m sensor aperture was dictated by the 40 m delay line and was designed to match the round-trip spacing between the localized point reflectors. This allowed us to monitor, in a single experiment, sensors formed using point reflectors, as shown in Fig. 2(b), and sensors formed using Rayleigh backscattering, as shown in Fig. 2(c). Also, note that by wrapping only 1 m of fiber on the PZT, we were able to monitor both a point-reflector based sensor and a Rayleigh-based sensor with apertures that contained the section of fiber wrapped on the PZT.

Note that this interrogation system could be simplified in the future. Using appropriate drive electronics, a single AOM could be used to both generate the pulse pair and introduce the frequency shift between the two pulses. Alternatively, by placing the path-mismatched

Optics EXPRESS

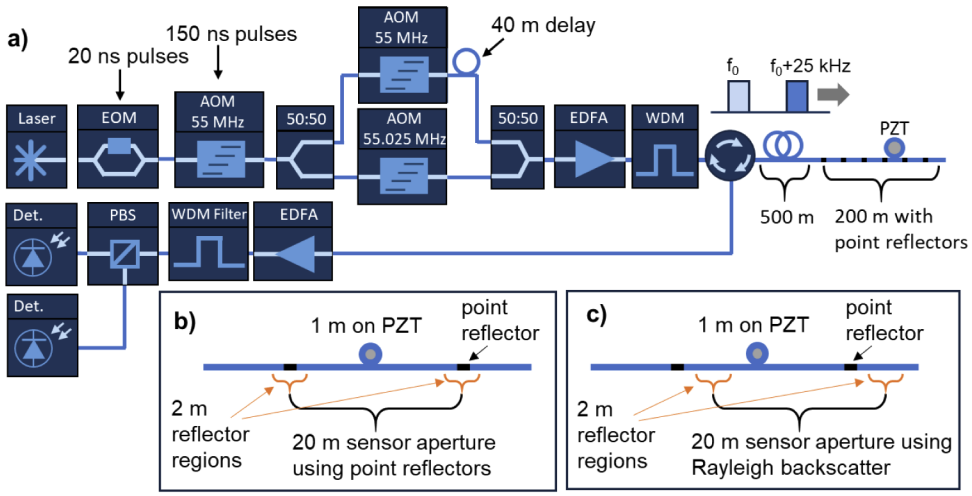

Fig. 2. (a) Experimental setup used to interrogate the EBF. A pair of 20 ns pulses with a frequency offset of 25 kHz was injected into the fiber under test. The Rayleigh backscattered light and light from the localized point reflectors was then directed to a polarization diversity receiver using a circulator and the interference between the two pulses was recorded using a high-speed digitizer. After demodulation, the system provides the relative phase between backscattered light from a pair of 2 m reflector regions separated by a 20 m sensing aperture at each position along the fiber. (b) In order to probe the strain induced by the PZT using a sensor formed with point reflectors, we select a location where the reflector regions are centered on neighboring point reflectors and the sensing aperture contains the length of fiber wrapped on the PZT. (c) The same PZT can also be probed by a sensor formed using Rayleigh backscattered light at a position where the reflector regions are offset from the point reflectors.

interferometer on the receive side, a baseband demodulation scheme could be used to maximize the sensor bandwidth [29].

4. Experimental performance characterization

Using the experimental setup shown in Fig. 2, we recorded a series of measurements while the PZT introduced varying levels of strain to the fiber. After digitization, the raw data was re-shaped to provide the interference signal at each position in the fiber over time (at an update rate of 100 kHz). The interference signal at each position in the fiber was then demodulated using the 25 kHz intermediate frequency between the pulses as a carrier. This provided the phase evolution over each sensor aperture in the fiber, as shown in Fig. 3(a). The PZT, which was located 790 m into the FUT, was driven at 2 kHz in this test and is clearly visible. We also calculated the power spectral density (PSD) of the sensor phase at each position in the fiber, as shown in Fig. 3(b). Again, the 2 kHz modulation signal at 790 m is visible. Note that the PZT modulation is visible over a ~20 m region. In this measurement, the phase shown at a given position represents the phase accumulated over a 20 m aperture centered at that location, as shown in Figs. 2(b) and 2(c). Thus, the PZT modulation is visible at any position within ±10 m of the PZT. Cross-sectional plots of the PSD at two positions in the fiber are shown in Fig. 3(c). These positions correspond to a sensor formed using either the 8^{th} and 9^{th} point reflectors (on either side of the PZT as shown in Fig. 2(b)) or a sensor formed using Rayleigh backscattered light on either side of the PZT, as shown in Fig. 2(c). Note that the strain introduced to the 1 m of fiber wrapped on the PZT

Optics EXPRESS

produced the same signal in both cases, as shown in in the inset of Fig. 3(c). In addition to producing the same signal as a standard Rayleigh-based sensor, the sensor formed with point reflectors also exhibited excellent linearity. This can be inferred from the PSD in Fig. 3(c), which shows a tone at 2 kHz with an SNR of ~60 dB without any evidence of harmonic distortion. As an additional test, we repeated this measurement while increasing the drive voltage applied to the PZT. The measured phase as a function of voltage is shown in Fig. 3(d), confirming that the sensor exhibits a high degree of linearity. We also plotted the PSD from a sensor formed after the PZT using the 9th and 10th point reflectors in Fig. 3(e). In this case, the 2 kHz signal was suppressed by 50 dB, confirming an excellent non-local signal rejection achieved using the double-pulse technique.

The main motivation for introducing the point reflectors is to achieve lower noise. This effect can be seen in Fig. 3(c), where the PSD obtained using the local reflectors shows ~20 dB lower noise than the PSD obtained using Rayleigh backscattered light at frequencies above 1 kHz. Below 1 kHz, the gradual increase in phase noise is due to environmental noise in the lab. The impact of the point reflectors is also evident in Fig. 3(b), in the form of ten parallel blue lines between 640 m and 820 m, revealing a series of positions in the fiber with low phase noise corresponding to the locations of the point reflectors. That is, these are positions where the reflector regions overlap with the point reflectors in the configuration shown in Fig. 2(b). To show this more clearly, we calculated the average PSD between 3 and 12 kHz (i.e. above the PZT drive frequency) at each position in the fiber, as shown in Fig. 4. We also plotted the reflected power at each position in the fiber in orange. As expected, the phase noise shows a series of minima at the locations of the point reflectors. The average phase noise of the sensors formed using point reflectors was −90.9 dB (re rad^2/Hz), compared with an average phase noise of −68.7 dB in the rest of the fiber where the sensors were formed using Rayleigh backscattered light. The minimum detectable strain noise can be calculated from the measured phase noise as $\sqrt{S_\varphi}\cdot[\lambda/(4\pi n\xi L)]$, where S_φ is the phase noise PSD, λ is the wavelength, n is the refractive index, ξ is the elasto-optic coefficient, and L is the sensor aperture [30]. Note that this expression assumes the strain is exerted uniformly across the entire sensor aperture. The minimum detectable strain for a 20 m sensor with a phase noise of −90.9 dB (re rad^2/Hz) is 0.15 $p\varepsilon/\sqrt{Hz}$.

In addition to providing lower noise, the standard deviation in the phase noise was reduced from 5.5 dB using Rayleigh backscattered light to 1.4 dB using the point reflectors. The significant variation in the phase noise formed using Rayleigh backscattered light is a characteristic of the intensity distribution of Rayleigh scattered light.

In addition to providing higher reflectance and enabling lower noise, the EBF also eliminates interference fading. Interference fading occurs when the Rayleigh backscattered light from a position in the fiber interferes destructively with itself. In a coherent φ-OTDR system, this fading can severely degrade the phase noise at certain positions in the fiber. This was evident in Fig. 4, which shows phase noise as much as 25 dB higher than the average level at some positions in the fiber. Moreover, as the temperature and strain in the fiber change over time, every position in the fiber will eventually experience interference fading. This can result in discontinuities in the measured phase (or strain) when the amplitude of the backscattered light approaches zero.

In order to confirm that the localized reflectors are immune to interference fading, we modulated the frequency of the seed laser. Changing the laser frequency has an analogous effect on the Rayleigh backscattered field as a change in temperature or strain [31]. Thus, by modulating the input frequency, we could controllably study the effect of changing the strain (or temperature) of the entire fiber under test.

In Fig. 5, we present the phase and amplitude of a typical sensor formed using Rayleigh backscattering and a sensor formed using point reflectors. These sensors were formed using the configurations shown in Figs. 2(b) and 2(c) so that both sensor apertures contained the 1 m region of fiber wrapped on the PZT In this measurement, the PZT was driven at 2 kHz, while the

Optics EXPRESS

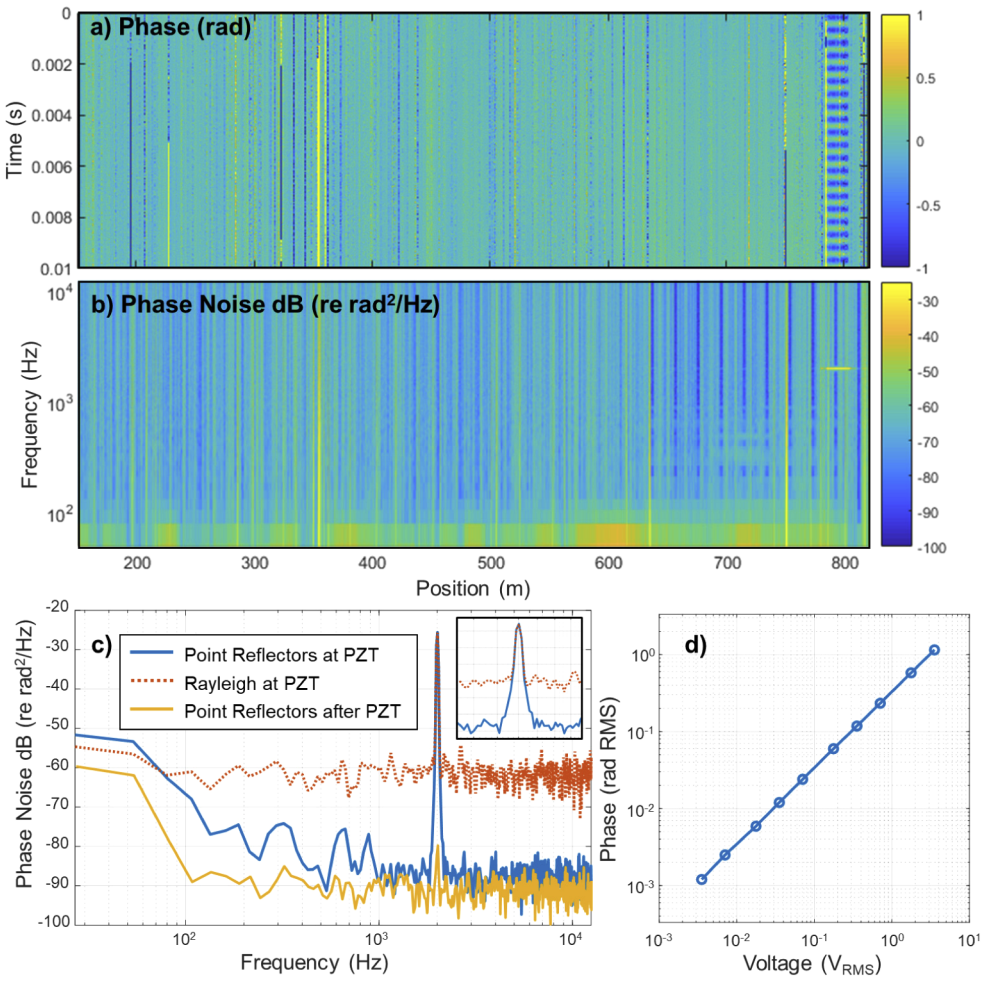

Fig. 3. (a) Measured phase at each position in the fiber. The PZT was located ~790 m into the fiber and driven at 2 kHz. (b) Phase noise PSD at each position in the fiber. The PZT modulation at 2 kHz is visible. In addition, the phase noise shows a series of minima corresponding to the positions of the point reflectors. (c) Phase noise PSD at three positions in the fiber, including a sensor formed using point reflectors covering the region of fiber wrapped on the PZT, a sensor formed using Rayleigh backscattering also covering the region of fiber wrapped on the PZT, and a sensor formed using point reflectors after the PZT. The PZT modulation produces the same signal level in the point reflector and Rayleigh based sensor without measurable harmonic distortion. The 2 kHz signal was suppressed by 50 dB in the sensor after the PZT. (d) The PZT-induced phase signal measured as a function of drive voltage using the point reflector sensor.

Optics EXPRESS

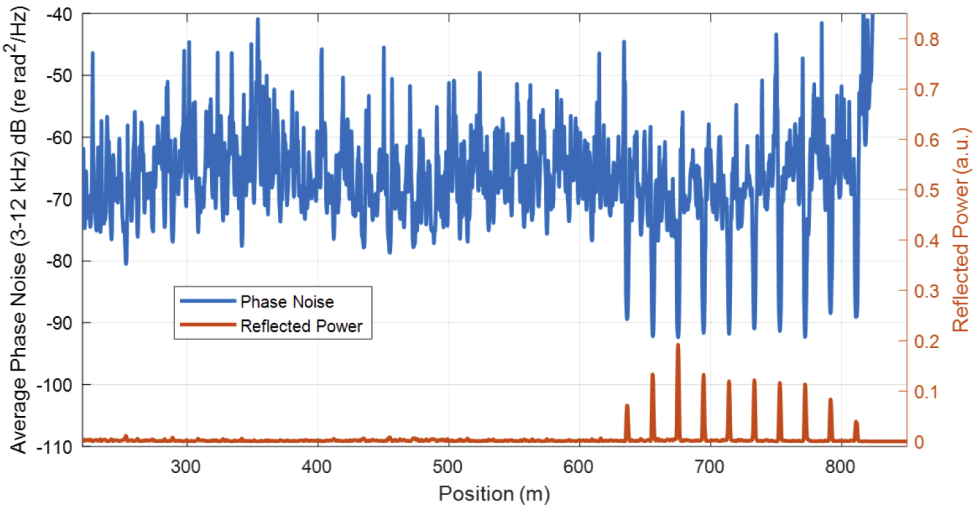

Fig. 4. Average phase noise between 3 and 12 kHz at each position in the fiber is shown in blue on the left-axis. The reflected power is shown in orange on the right axis. The sensors formed using the point reflectors exhibited an average phase noise of −90.9 dB (re rad^2/Hz) compared with an average noise of −68.7 (re rad^2/Hz) dB in the rest of the fiber.

laser frequency was modulated at 100 Hz with a deviation of 10 MHz. The amplitude of the Rayleigh backscattered light, shown in Fig. 5(a), is clearly impacted by the 100 Hz frequency modulation. In addition, the measured phase changes discontinuously when the backscattered amplitude approaches a local minimum. In contrast, the amplitude of the return light from the localized reflectors is nearly constant despite the laser frequency modulation, as shown in Fig. 5(b). Moreover, the sensor formed using point reflectors accurately measures the phase imparted by the PZT for the duration of the measurement. This measurement, combined with our observations over a series of similar experiments, confirmed that the sensors formed using point reflectors are effectively immune to interference fading.

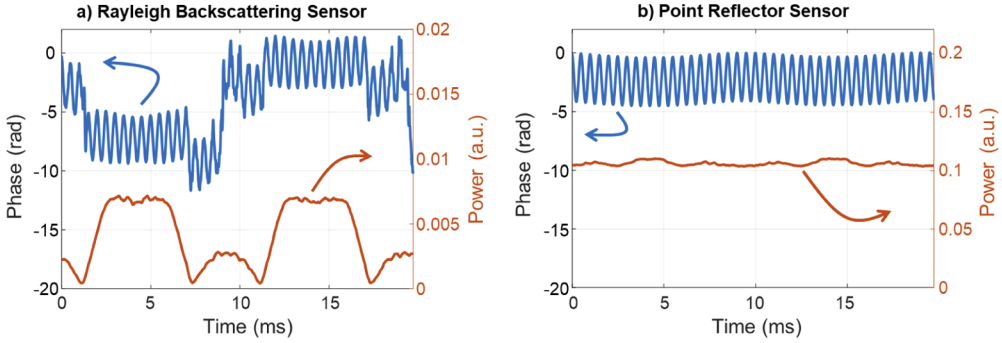

Fig. 5. (a) Phase and amplitude of a sensor formed using Rayleigh backscattered light covering the PZT region. The laser frequency modulation impacted the backscattered amplitude and the measured phase exhibited discontinuities when the amplitude approached a minima, indicative of interference fading. (b) The phase and amplitude of a sensor formed using point reflectors. The laser frequency modulation had minimal impact on the reflected power and the phase modulation imparted by the PZT was successfully recovered for the entire measurement.

Optics EXPRESS

5. Conclusion

In summary, we presented a low-noise DAS based on enhanced backscattering fiber. The fiber was fabricated in a fully automated system by focusing an ultra-fast laser through the cladding of standard telecom fiber to add a series of point reflectors. The point reflectors had an average reflectance of −53 dB and we found that 100 reflectors introduced ~0.01 dB of attenuation. Using a coherent φ-OTDR system, we showed that the point reflectors enabled a phase noise of −90 dB (re rad^2/Hz) compared with a noise floor of −69 dB (re rad^2/Hz) obtained using Rayleigh backscattered light. The sensor exhibited a high degree of linearity and excellent non-local signal suppression. The sensor is also immune to interference fading, enabling the use of a relatively simple, single wavelength interrogation system. This work opens us a new path to low-noise DAS using micro-machined fiber.

Funding

U.S. Naval Research Laboratory; Natural Environment Research Council (NE/S012877/1); Royal Society (CHL\R1\180350).

Disclosures

The authors declare no conflicts of interest.

References

1. A. Masoudi and T. P. Newson, "Contributed Review: Distributed optical fibre dynamic strain sensing," Rev. Sci. Instrum. **87**(1), 011501 (2016).
2. J. C. Juarez and H. F. Taylor, "Field test of a distributed fiber-optic intrusion sensor system for long perimeters," Appl. Opt. **46**(11), 1968–1971 (2007).
3. F. Peng, H. Wu, X.-H. Jia, Y.-J. Rao, Z.-N. Wang, and Z.-P. Peng, "Ultra-long high-sensitivity Φ-OTDR for high spatial resolution intrusion detection of pipelines," Opt. Express **22**(11), 13804–13810 (2014).
4. A. Masoudi, J. A. Pilgrim, T. P. Newson, and G. Brambilla, "Subsea Cable Condition Monitoring with Distributed Optical Fiber Vibration Sensor," J. Lightwave Technol. **37**(4), 1352–1358 (2019).
5. H. Izumita, S. Furukawa, Y. Koyamada, and I. Sankawa, "Fading Noise Reduction in Coherent OTDR," IEEE Photonics Technol. Lett. **4**(2), 201–203 (1992).
6. J. Zhou, Z. Pan, Q. Ye, H. Cai, R. Qu, and Z. Fang, "Characteristics and Explanations of Interference Fading of a φ-OTDR With a Multi-Frequency Source," J. Lightwave Technol. **31**(17), 2947–2954 (2013).
7. J. C. Juarez and H. F. Taylor, "Polarization discrimination in a phase-sensitive optical time-domain reflectometer intrusion-sensor system," Opt. Lett. **30**(24), 3284–3286 (2005).
8. M. Zabihi, Y. Chen, T. Zhou, J. Liu, Y. Shan, Z. Meng, F. Wang, Y. Zhang, X. Zhang, and M. Chen, "Continuous Fading Suppression Method for Φ-OTDR Systems Using Optimum Tracking Over Multiple Probe Frequencies," J. Lightwave Technol. **37**(14), 3602–3610 (2019).
9. A. H. Hartog, L. B. Liokumovich, N. A. Ushakov, O. I. Kotov, T. Dean, T. Cuny, A. Constantinou, and F. V. Englich, "The use of multi-frequency acquisition to significantly improve the quality of fibre-optic-distributed vibration sensing," Geophys. Prospect. **66**(S1), 192–202 (2018).
10. L. Costa, H. F. Martins, S. Martin-Lopez, M. R. Fernandez-Ruiz, and M. Gonzalez-Herraez, "Fully Distributed Optical Fiber Strain Sensor With 10 −12 $\varepsilon/\sqrt{\text{Hz}}$ Sensitivity," J. Lightwave Technol. **37**(18), 4487–4495 (2019).
11. D. Chen, Q. Liu, Y. Wang, H. Li, and Z. He, "Fiber-optic distributed acoustic sensor based on a chirped pulse and a non-matched filter," Opt. Express **27**(20), 29415–29424 (2019).
12. S. Liehr, S. Münzenberger, and K. Krebber, "Wavelength-scanning coherent OTDR for dynamic high strain resolution sensing," Opt. Express **26**(8), 10573–10588 (2018).
13. B. Redding, M. J. Murray, A. Davis, and C. K. Kirkendall, "Quantitative amplitude measuring ϕ-OTDR using multiple uncorrelated Rayleigh backscattering realizations," Opt. Express **27**(24), 34952–34960 (2019).
14. S. Loranger, M. Gagné, V. Lambin-Iezzi, and R. Kashyap, "Rayleigh scatter based order of magnitude increase in distributed temperature and strain sensing by simple UV exposure of optical fibre," Sci. Rep. **5**(1), 11177 (2015).
15. A. Yan, S. Huang, S. Li, R. Chen, P. Ohodnicki, M. Buric, S. Lee, M. J. Li, and K. P. Chen, "Distributed Optical Fiber Sensors with Ultrafast Laser Enhanced Rayleigh Backscattering Profiles for Real-Time Monitoring of Solid Oxide Fuel Cell Operations," Sci. Rep. **7**(1), 9360 (2017).
16. Y. Xu, P. Lu, S. Gao, D. Xiang, P. Lu, S. Mihailov, and X. Bao, "Optical fiber random grating-based multiparameter sensor," Opt. Lett. **40**(23), 5514–5517 (2015).
17. F. Monet, S. Loranger, V. Lambin-Iezzi, A. Drouin, S. Kadoury, and R. Kashyap, "The ROGUE: a novel, noise-generated random grating," Opt. Express **27**(10), 13895–13909 (2019).

Optics EXPRESS

18. P. S. Westbrook, T. Kremp, K. S. Feder, W. Ko, E. M. Monberg, H. Wu, D. A. Simoff, T. F. Taunay, and R. M. Ortiz, "Continuous multicore optical fiber grating arrays for distributed sensing applications," J. Lightwave Technol. **35**(6), 1248–1252 (2017).
19. P. S. Westbrook, K. S. Feder, R. M. Ortiz, T. Kremp, E. M. Monberg, H. Wu, D. A. Simoff, and S. Shenk, "Kilometer length low loss enhanced back scattering fiber for distributed sensing," in *25th International Conference on Optical Fiber Sensors* (IEEE, 2017), p. 17012426.
20. G. Cedilnik, G. Lees, P. E. Schmidt, S. Herstrom, and T. Geisler, "Pushing the Reach of Fiber Distributed Acoustic Sensing to 125 km Without the Use of Amplification," IEEE Sens. Lett. **3**(3), 1–4 (2019).
21. C. Wang, Y. Shang, X.-H. Liu, C. Wang, H.-H. Yu, D.-S. Jiang, and G.-D. Peng, "Distributed OTDR-interferometric sensing network with identical ultra-weak fiber Bragg gratings," Opt. Express **23**(22), 29038–29046 (2015).
22. F. Zhu, Y. Zhang, L. Xia, X. Wu, and X. Zhang, "Improved Φ-OTDR sensing system for high-precision dynamic strain measurement based on ultra-weak fiber bragg grating array," J. Lightwave Technol. **33**(23), 4775–4780 (2015).
23. M. Wu, X. Fan, Q. Liu, and Z. He, "Highly sensitive quasi-distributed fiber-optic acoustic sensing system by interrogating a weak reflector array," Opt. Lett. **43**(15), 3594–3597 (2018).
24. J. Wu, Z. Peng, M. Wang, R. Cao, M. J. Li, H. Wen, H. Liu, and K. P. Chen, "Fabrication of Ultra-Weak Fiber Bragg Grating (UWFBG) in Single-Mode Fibers through Ti-Doped Silica Outer Cladding for Distributed Acoustic Sensing," in *Optical Sensors and Sensing Congress* (OSA, 2019), p. ETh1A.4.
25. H. Guo, F. Liu, Y. Yuan, H. Yu, and M. Yang, "Ultra-weak FBG and its refractive index distribution in the drawing optical fiber," Opt. Express **23**(4), 4829–4838 (2015).
26. A. Donko, R. Sandoghchi, A. Masoudi, M. Beresna, and G. Brambilla, "Low-Loss Micro-Machined Fiber With Rayleigh Backscattering Enhanced By Two Orders Of Magnitude," in *OFS Conference Proceedings* (OSA, 2018), p. WF75.
27. Z. Peng, J. Jian, H. Wen, M. Wang, H. Liu, D. Jiang, Z. Mao, and K. P. Chen, "Fiber-optical distributed acoustic sensing signal enhancements using ultrafast laser and artificial intelligence for human movement detection and pipeline monitoring," Proc. SPIE **10937**, 109370J (2019).
28. A. D. Kersey, K. L. Dorsey, and A. Dandridge, "Cross talk in a fiber-optic Fabry–Perot sensor array with ring reflectors," Opt. Lett. **14**(1), 93–95 (1989).
29. R. Posey, G. A. Johnson, and S. T. Vohra, "Strain sensing based on coherent Rayleigh scattering in an optical fibre," Electron. Lett. **36**(20), 1688–1689 (2000).
30. C. K. Kirkendall and A. Dandridge, "Overview of high performance fibre-optic sensing," J. Phys. D: Appl. Phys. **37**(18), R197–R216 (2004).
31. Y. Koyamada, M. Imahama, K. Kubota, and K. Hogari, "Fiber-optic distributed strain and temperature sensing with very high measurand resolution over long range using coherent OTDR," J. Lightwave Technol. **27**(9), 1142–1146 (2009).